



<http://www.diva-portal.org>

This is the published version of a paper published in *AIP Advances*.

Citation for the original published paper (version of record):

Abbasiasl, T., Niazi, S., Sheibani Aghdam, A., Chen, H., Cebeci, F C. et al. (2020)  
Effect of intensified cavitation using poly (vinyl alcohol) microbubbles on spray  
atomization characteristics in microscale  
*AIP Advances*

Access to the published version may require subscription.

N.B. When citing this work, cite the original published paper.







Permanent link to this version:

<http://urn.kb.se/resolve?urn=urn:nbn:se:kth:diva-268892>

# Effect of intensified cavitation using poly(vinyl alcohol) microbubbles on spray atomization characteristics in microscale

Cite as: AIP Advances **10**, 025318 (2020); <https://doi.org/10.1063/1.5142607>

Submitted: 16 December 2019 . Accepted: 28 January 2020 . Published Online: 12 February 2020

Taher Abbasiasl , Soroush Niazi , Araz Sheibani Aghdam, Hongjian Chen , Fevzi Çakmak Cebeci , Morteza Ghorbani , Dmitry Grishenkov, and Ali Koşar 



View Online



Export Citation



CrossMark

## ARTICLES YOU MAY BE INTERESTED IN

[Energy harvesting with micro scale hydrodynamic cavitation-thermoelectric generation coupling](#)

AIP Advances **9**, 105012 (2019); <https://doi.org/10.1063/1.5115336>

[Increasing the stability of nanofluids with cavitating flows in micro orifices](#)

Applied Physics Letters **109**, 104101 (2016); <https://doi.org/10.1063/1.4962330>

[Biomedical device prototype based on small scale hydrodynamic cavitation](#)

AIP Advances **8**, 035108 (2018); <https://doi.org/10.1063/1.5005048>

## AVS Quantum Science

Co-Published by



RECEIVE THE LATEST UPDATES



# Effect of intensified cavitation using poly(vinyl alcohol) microbubbles on spray atomization characteristics in microscale

Cite as: AIP Advances 10, 025318 (2020); doi: 10.1063/1.5142607

Submitted: 16 December 2019 • Accepted: 28 January 2020 •

Published Online: 12 February 2020



Taher Abbasiasl,<sup>1,2</sup> Sorous Niazi,<sup>1,2</sup> Araz Sheibani Aghdam,<sup>2</sup> Hongjian Chen,<sup>3</sup> Fevzi Çakmak Cebeci,<sup>1,2</sup> Morteza Ghorbani,<sup>1,2,3</sup> Dmitry Grishenkov,<sup>3</sup> and Ali Koşar<sup>1,2,4,a)</sup>

## AFFILIATIONS

<sup>1</sup>Sabancı University Nanotechnology Research and Application Center, 34956 Tuzla, Istanbul, Turkey

<sup>2</sup>Faculty of Engineering and Natural Science, Sabancı University, 34956 Tuzla, Istanbul, Turkey

<sup>3</sup>Department of Biomedical Engineering and Health Systems, KTH Royal Institute of Technology, SE-141 57 Stockholm, Sweden

<sup>4</sup>Center of Excellence for Functional Surfaces and Interfaces for Nano-Diagnostics (EFSUN), Sabancı University, Orhanlı, 34956 Tuzla, Istanbul, Turkey

<sup>a)</sup> Author to whom correspondence should be addressed: [kosara@sabanciuniv.edu](mailto:kosara@sabanciuniv.edu)

## ABSTRACT

In this study, cavitating flows inside a transparent cylindrical nozzle with an inner diameter of 0.9 mm were visualized, and the effect of cavitation on atomization characteristics of emerging sprays was investigated. Different patterns of cavitating flows inside the nozzle were visualized using a high-speed camera. In-house codes were developed to process the captured images to study the droplet size distribution and droplet velocity in different flow regimes. The results show that cavitating flows at the microscale have significant effects on atomization characteristics of the spray. Two working fluids, namely, water and poly(vinyl alcohol) microbubble (PVA MB) suspension, were employed. Accordingly, the injection pressures were detected as 690 kPa, 1035 kPa, and 1725 kPa for cavitation inception, supercavitation, and hydraulic flip flow regimes in the case of water, respectively. The corresponding pressures for the aforementioned patterns for PVA MB suspension were 590 kPa, 760 kPa, and 1070 kPa, respectively. At the microscale, as a result of a higher volume fraction of cavitation bubbles inside the nozzle, there is no large difference between the cavitation numbers corresponding to cavitating and hydraulic flip flows. Although the percentage of droplets with diameters smaller than 200  $\mu\text{m}$  was roughly the same for both cases of water and PVA MB suspension, the Sauter mean diameter was considerably lower in the case of PVA MBs. Moreover, higher droplet velocities were achieved in the case of PVA MBs at lower injection pressures.

© 2020 Author(s). All article content, except where otherwise noted, is licensed under a Creative Commons Attribution (CC BY) license (<http://creativecommons.org/licenses/by/4.0/>). <https://doi.org/10.1063/1.5142607>

## I. INTRODUCTION

The cavitation phenomenon results in phase change inside liquid and formation of several bubbles, and it has significant effects on many processes such as atomization and break-up of the liquid jet.<sup>1</sup> Understanding the behavior of cavitating flow regimes in the microscale is a challenging task, and the amount of related data in the literature is not as abundant as that corresponding to macro- or miniscale. In this regard, Mishra and Peles<sup>2</sup> experimentally investigated hydrodynamic cavitation in a short microchannel,

and they showed that the cavitation phenomenon was different at the microscale. There are also some numerical studies about cavitating flows at the microscale.<sup>3,4</sup> The collapse of cavitation bubbles at the outlet of the nozzle enhances spray atomization. Therefore, researchers attempt to move the cavitation bubbles to the end of the nozzle to reduce the length of liquid jet just after the nozzle. According to the studies by Payri and co-workers, cavitating flows lead to a rise in the spray cone angle as well as in the speed of the injected flow.<sup>5,6</sup> During the past decade, several studies have focused on the cavitation phenomenon inside transparent nozzles

and its impact on spray characteristics.<sup>7–10</sup> For example, Suh and Lee<sup>11</sup> investigated the impact of cavitation on diesel fuel atomization in 2D transparent acrylic resin nozzles with different length to width ratios. They studied the flow inside the nozzle and the spray morphology under different experimental conditions. There are other similar studies on the importance of cavitation and its effect on spray characteristics.<sup>7,12</sup>

To be able to exploit the effect of cavitation on spray formation, it is crucial to have a better understanding about the atomization quality, droplet size, cone angle, and other important parameters of the spray. For this purpose, several experimental and numerical studies have concentrated on the effect of cavitating flows on spray formation over a wide variety of operating conditions.<sup>13–16</sup> In this regard, Nurick<sup>17</sup> proposed an experimental model to explain the behavior of the discharge coefficient within sharp-edged circular and rectangular orifices. The mixing uniformity of spray was established under different conditions, during cavitating and non-cavitating flows. Cavitation was shown to reduce the mixing uniformity for circular orifice elements. Since most of the atomization nozzles are of micro- or miniscale (tens to several hundred micrometers), it is a challenging task to optically investigate cavitating flows inside the nozzle and its effect on the spray. As a result, there are numerous numerical studies on cavitating flows in nozzles and its impact on the atomization quality of sprays. Örley *et al.*<sup>18</sup> performed a large eddy simulation of cavitating flows inside rectangular nozzles. They did their numerical study based on the experimental configuration of Sou *et al.*<sup>12</sup> There was a good agreement between the simulation and experimental results. According to the numerical results, the main mechanisms, which promote primary break-up, are turbulent fluctuations caused by the collapse of cavitation bubbles near the nozzle exit, gas entrainment into the nozzle, and collapse events inside the liquid jet adjacent to the liquid gas interface.

Most of the experimental studies focusing on the effect of cavitating flows on jet atomization and spray characteristics have utilized 2D rectangular nozzles so that they could allow visualization of cavitating flows inside nozzles. As a result, there is still a considerable lack of information on the influence of cavitation inside 3D nozzles (e.g., cylindrical nozzles) on spray formation. Some studies employed nozzles with circular cross sections to investigate different stages of cavitation development inside the nozzle. However, they did not offer any noticeable information about the atomization features of sprays.<sup>9,19</sup>

The majority of studies on the transition from liquid jet to spray with separated droplets considered flow regimes inside the macroscale nozzles to examine the impact of cavitation on the spray performance,<sup>7,11,12,19–21</sup> while the number of studies focusing on the effect of cavitating flows inside micro-nozzles on spray properties is rather scarce.<sup>10,14,22</sup> Besides, in most of the investigations on spray behavior in microscale, there are limited visualization efforts for observing the development of cavitating flows inside nozzles, and the captured images are not very clear to distinguish different stages of cavitation and its effect on liquid jets and atomization of sprays.<sup>22–25</sup>

In order to intensify the cavitating flows of water inside nozzles and to reduce the required injection pressure for cavitation inception, some studies proposed roughened surfaces<sup>26</sup> and droplets<sup>27</sup> or microbubbles<sup>26</sup> in the working fluid. Aghdam *et al.*<sup>28</sup> modified the inner surface of microchannels using layer-by-layer (LBL)

assembled Slippery Liquid-Infused Porous Surfaces (SLIPS). This technique of surface modification significantly reduced the inception pressure. Moreover, in the roughened microchannel, supercavitation conditions could be achieved for all the microchannels at lower upstream pressure, whereas supercavitation conditions did not occur for a number of microchannels in the same range of upstream pressures for the non-roughened surfaces. Ghorbani *et al.*<sup>26</sup> implemented both roughened microchannels and microbubbles [poly(vinyl alcohol) microbubbles] for the purpose of intensifying cavitation and lowering the required pressure for cavitation inception. They achieved promising results in this regard.

Even though the dominant role of supercavitation in changing the flow regimes inside micro/macro channels has been already shown,<sup>12,19,29</sup> there is still a lack of information about the effect of supercavitation on sprays. For example, while Suh and Lee<sup>11</sup> compared atomization characteristics of sprays in cavitating and turbulent flows, the effect of supercavitation was not discussed in that study. There are some studies addressing the impact of supercavitation on sprays; however, they did not offer detailed data related to droplet count, size distribution, and velocity.<sup>4,7</sup> In their study, Li *et al.*<sup>30</sup> investigated the effect of cavitating flows inside a micro-size single-hole diesel injector on sprays; nevertheless, they did not provide sufficient information about atomization characteristics.

In this study, first, cavitating flows inside a micro-nozzle made of transparent quartz are visualized, and the effect of cavitation on emerging spray is investigated in terms of atomization characteristics and velocity of the departed droplets. Then, inspired by the above-mentioned studies, water suspensions of poly(vinyl alcohol) microbubbles (PVA MBs) are employed as another working fluid to study the effect of intensified cavitation on the properties of the spray. This study illustrates the potential of PVA MBs as cheap, stable, chemically versatile, and non-toxic suspensions in spray atomization. Moreover, the inner surface of the nozzle is also roughened to further intensify cavitation and to lower the required injection pressure for cavitation inception. Enhanced atomization characteristics of the spray are achieved as a result of cavitating flows and by using PVA MBs suspension inside the nozzle with surface roughness enhanced cavitation. The dominant role of supercavitation in atomization properties of the emerging spray is also discussed in detail.

## II. EXPERIMENTAL APPARATUS AND PROCEDURE

### A. Experimental apparatus

Figure 1 shows a schematic of the experimental setup. A high-pressure nitrogen tank was used to provide the desired injection pressure of the working fluid. A micro-filter was employed to eliminate the particles larger than 15  $\mu\text{m}$  from the liquid. Pressure gauges were placed at different locations of the system to monitor the pressure. One pressure gauge was mounted immediately before the nozzle in order to measure the injection pressure of the working fluid. All the parts before the transparent tube were made of stainless steel to avoid any chemical reaction with the working fluid. The nozzle was made of transparent quartz to allow the visualization of cavitating flows inside the nozzle. The geometry of the quartz nozzle is illustrated in Fig. 2, and the detailed dimensions of the nozzle are presented in Table I. The inner and outer diameters of the first part of the nozzle were exactly the same as the stainless-steel tube to have

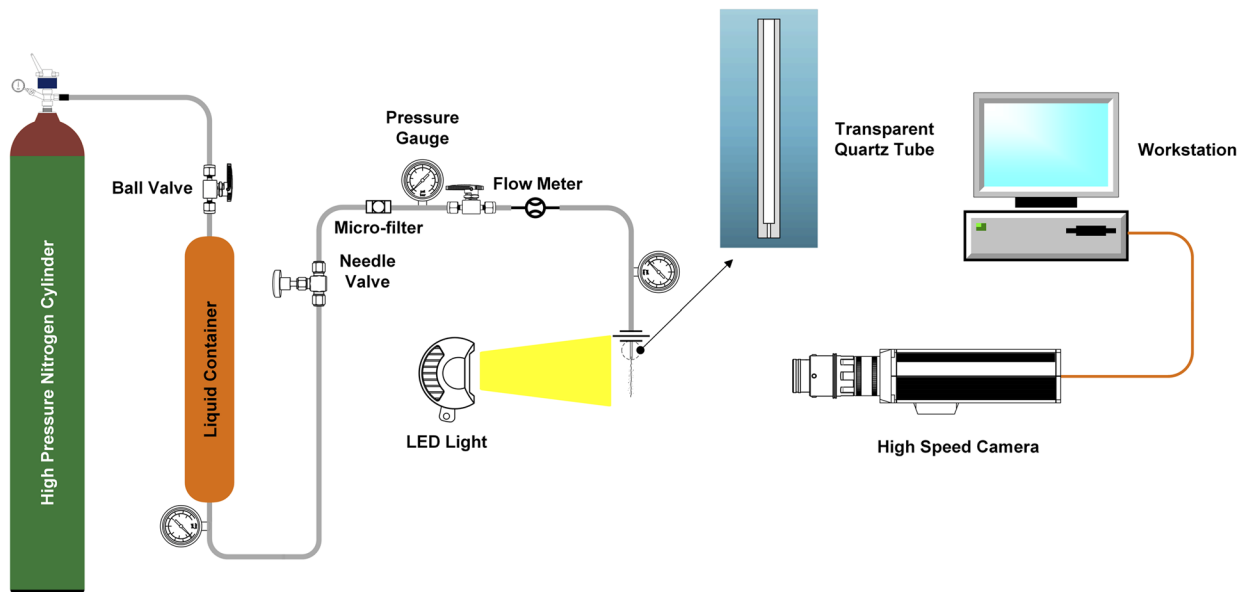


FIG. 1. Schematic of the experimental setup.

negligible pressure losses along the experimental setup. Before performing the experiments, in order to minimize the gas content in the working fluid, degassing was performed by exposing the working fluids to vacuum. The first part of the quartz tube was long enough to provide sufficient time for observing the working fluid and to make sure that there was no undesired disturbance in the working fluid before entering the nozzle (Fig. 2). The experiments were conducted at ambient pressure of 1 atm and a temperature of 293 K. Various injection pressures were tested to investigate the cavitating flow inside the nozzle.

A high-speed camera (Phantom V9.1) was used to the capture real-time images of cavitating flows as well as liquid jets, and a Veritas miniConstellation 120.28° light-emitting diode (LED) light source was employed as the illumination system. The light source

generated white light flashes, and the pulse duration could be as short as 2  $\mu$ s with a maximum pulse rate of 100 kHz. The shadowgraphy method was implemented to observe the flows inside the transparent nozzle and its effect on the emerged spray. The high-speed camera was connected to a personal computer (PC) to record the real-time images of the experiments using PCC software version 3.4.788.0 (AMETEK, Inc., Berwyn, PA). The resolution of the captured images was 1280  $\times$  800 pixel for cavitation visualization inside the nozzle. However, for the spray studies, the resolution of the 192  $\times$  192 pixel was chosen to be able to capture the droplets with high velocity as clear as possible. The exposure time was adjusted to the value of 2  $\mu$ s.

B. Surface modification

The inner surface of the nozzle part of the tubes was treated to have SLIPS (Slippery Liquid Induced Porous Surfaces) coatings to enhance cavitating flows and to reduce the probability of the collapse of the bubbles, which are generated upon cavitation, before leaving the nozzle.<sup>28</sup> For this purpose, by using the layer-by-layer (LBL) assembly technique, five by layers of positively charged poly(allylamine hydrochloride) with an average molecular weight of 50 000 (PAH) and negatively charged poly(sodium 4-styrenesulfonate) with an average molecular weight of 70 000 (SPS) were assembled on the surface of the nozzle, and, then, 10 by layers of PAH polyelectrolyte and homemade silica nanoparticles with 40 nm and 80 nm in diameter were deposited on the surface of the nozzle. The LBL assemblies were applied using the fluidic assembly technique as described in our previous work.<sup>27</sup> The affinity of the surface was modified using 1H,1H,2H,2H-perfluorodecyltriethoxysilane 97% (PFDTs), which was applied by chemical vapor deposition and was followed by heat treatment to increase the stability of the fluorinated surface. Finally, the Slippery

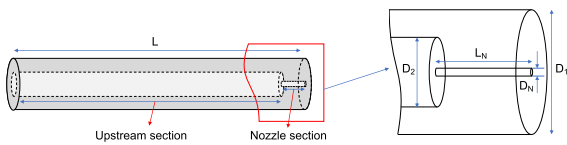
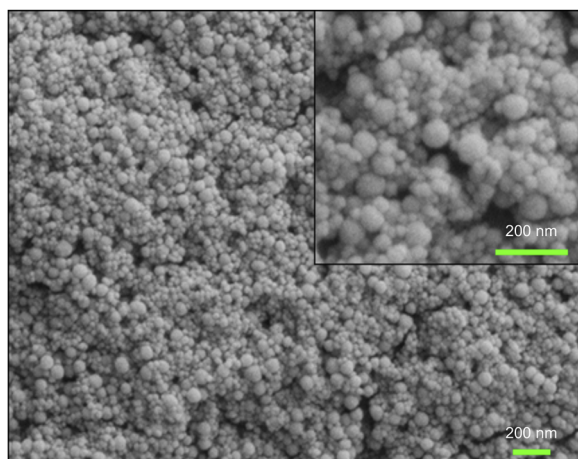


FIG. 2. Schematic of the test nozzle.

TABLE I. Detailed specifications of the test nozzle.

L (total length of the quartz tube)	6 cm
L <sub>N</sub> (length of the nozzle section of the tube)	4 mm
D <sub>1</sub> (outer diameter of the tube)	6.35 mm
D <sub>2</sub> (inner diameter of the upstream section of the tube)	3.05 mm
D <sub>N</sub> (inner diameter of the nozzle part of the tube)	0.9 mm



**FIG. 3.** SEM image of the layer-by-layer assembled surface on a quartz plate.

Liquid-Infused Porous Surfaces (SLIPS) were formed by entrapping a fluorinated lubricant within the pores of the assembled surface. The surface modification increases the chance of the Fomblin YLVAC 25/6 with an average molecular weight of 3300 (PFPE) to be trapped within the pores of the surface. SEM (Scanning Electron Microscopy) image of the LBL assembled surface on a quartz plate is shown in Fig. 3. The detailed description of the surface modification process and achieving SLIPS was described in our preview studies.<sup>27,28</sup>

The AFM results of smooth and rough surfaces are included in Table II. The peak to peak roughness of the rough surface is six times the smooth ones. The projected surface shows the surface increase due to the increased roughness. Accordingly, the projected surface for the rough surface reaches 12.8%. The Rq or rms value of the rough surfaces is 30 times more than the smooth ones.

### C. Protocol for PVA MB fabrication

The fabrication protocol of PVA MBs was described by Cavaliere *et al.*<sup>31</sup> 4 g of PVA was dissolved in 200 ml MilliQ-water and was heated up to 80 °C. 380 mg of NaIO<sub>4</sub> was added into the solution to form telechelic PVA at a temperature of 80 °C for 1 h. The telechelic PVA solution was then cooled down to room temperature. A homogenizer (UltraTurrax, IKA, Königswinter, Germany)

**TABLE II.** The AFM results of smooth and modified surfaces. (Superscripts: 1. Height difference between the maximum and minimum, 2. Surface area difference between the actual and projected surfaces, 3. Root mean square roughness of the surface, 4. Arithmetic average of the absolute values of the roughness).

	Smooth surface	Rough surface
Z range <sup>1</sup> (nm)	13.2	97.4
Surface % <sup>2</sup>	0.423	12.8
Rq <sup>3</sup> (nm)	0.583	15.3
Ra <sup>4</sup> (nm)	0.427	12.2

equipped with a stainless-steel tip S 25 N - 25 G (UltraTurrax, IKA, Königswinter, Germany) was employed to apply shearing force at the air/water interface of the telechelic PVA solution to cross-link the telechelic PVA under room temperature for 2 h. The resulting PVA MBs were harvested and washed 10 times. The PVA MBs have relatively a narrow size distribution below 10 μm with an average diameter (normalized by volume) of  $3.5 \mu\text{m} \pm 0.77 \mu\text{m}$  and a concentration of  $2.72 \times 10^8 \text{ ml}^{-1}$ . The volume fraction of the master suspension is estimated as  $3.5 \times 10^{-4}$ .

In our study, an aqueous suspension of stable air-filled microbubbles was prepared at room temperature and at pH 5 using 2% W/V telechelic PVA aqueous solution. The surface tension of 2% PVA solution is approximately 0.055 N/m.<sup>32</sup> The density of the PVA powder used in our study is 1269 kg/m<sup>3</sup>.<sup>33</sup> The vapor pressure of water in the PVA aqueous solution is 3.54 kPa,<sup>34</sup> while the vapor pressure of pure water is 2.33 kPa. The higher value of the vapor pressure for the PVA aqueous solution results in the earlier arrival of the cavitation inception for the case of PVA suspension.

PVA microbubbles were prepared separately and then injected into the system for testing. PVA alone is a water-soluble powder, which is not the subject of the manuscript. Microbubbles with the PVA shell were suspended in water. All PVA fragments or broken, formed, or unformed shells were removed from the fabrication solution during the 10 day filtering procedure using a separation funnel. The fabrication and filtering protocol and complete physical characteristics of the PVA MBs were reported in our previous study.<sup>26</sup>

The PVA MBs will float to the top if the suspension stands still. Moreover, the PVA MBs have a high echogenicity under ultrasound imaging. Such pieces of evidence suggest that the PVA MBs have a core with low density, great mechanical impedance mismatch with solid (liquid), and a high compressibility. Therefore, the core of MBs cannot be solid or liquid; it must be gas. Furthermore, Kothapalli *et al.* (Kothapalli *et al.* 2015) reported the pumping-out fracturing mechanism of PVA MBs.<sup>35</sup> They observed that under a high pressure ultrasound wave, the shell of MBs cracked and the gas of PVA MB core leaked out from a shell-less bubble and finally dissolved in water.

The size of PVA MBs was obtained by a microscope in this study. Similar results were obtained by confocal laser microscopy<sup>36</sup> and dynamic light scattering.<sup>37</sup>

### D. Experimental procedure

Water and PVA MB suspensions were used as the working fluids to study the effect of cavitation on flow inside the nozzle and spray atomization. The physical properties of PVA MB suspensions are included in Table III.

**TABLE III.** Physical properties of the working fluid.

Working fluid	Suspension of PVA MBs
Temperature (K)	293
Density (kg·m <sup>-3</sup> )	1269
Viscosity (mPa·s)	1.00
Vapor pressure (kPa)	3.54



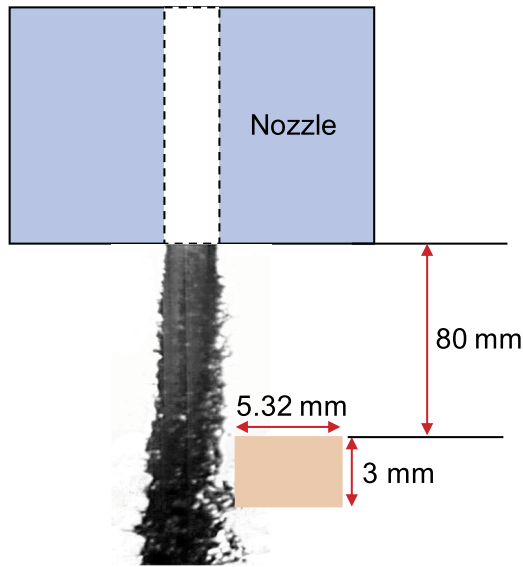


**FIG. 4.** Position of the window used for spray visualization during droplet measurements.

Experiments were conducted under various test conditions [various Reynolds numbers ( $Re$ ) and cavitation numbers ( $\sigma$ )]. Cavitation number, which is an indicator of the intensity of cavitation, is defined as

$$\sigma = \frac{P_i - P_v}{(\rho V^2/2)}, \quad (1)$$

where  $P_i$ ,  $P_v$ ,  $\rho$ , and  $V$  are the injection pressure, vapor pressure, density of the working fluid, and velocity in the nozzle, respectively. The velocity of the fluid is the ratio of the flow rate to cross-sectional area of the nozzle.

Reynolds number is defined as

$$Re = \frac{\rho V D}{\mu}, \quad (2)$$

where  $D$  and  $\mu$  are the nozzle diameter and viscosity of the working fluid, respectively.

Sauter mean diameter (SMD), which is used in atomization studies, is defined as

$$D_{32} = \frac{\sum n_i d_i^3}{\sum n_i d_i^2}, \quad (3)$$

where  $D_{32}$  is the Sauter mean diameter (SMD),  $n_i$  is the number of droplets in the size range  $i$ , and  $d_i$  is the diameter of droplet in the size range  $i$ .

### E. Image processing

In order to obtain spray atomization characteristics and the effect of cavitation on the droplet size and velocity distribution, spray visualization experiments were conducted at a location as near as possible to the emerging liquid jet.<sup>11</sup> Figure 4 demonstrates the precise location of the window with respect to the nozzle and liquid jet, which was used to capture images for the droplet size and velocity calculations. For water experiments, four injection pressures corresponding to four different flow regimes inside the nozzles were chosen to investigate the atomization characteristics, namely, (1) non-cavitating flow, (2) cavitation inception, (3) developed cavitation, and (4) supercavitation. According to the results of the atomization study in the case of water (Sec. III C), supercavitation has the dominant effect on enhancing atomization, and as a result, the atomization study was not performed for developed cavitation of PVA MB suspension. Spray was observed with a sampling speed of 24 096 images per second. For droplet size distribution at different pressures, 250 frames with a time difference of 830  $\mu$ s were selected so that the time difference between the frames could be long enough to avoid appearance of the same droplet on two different frames. The selected images were processed using an in-house developed code in MATLAB<sup>TM</sup> 2018a (MathWorks, Inc., Natick, MA) to recognize the droplets on each frame and to determine their diameters. For better understanding of the droplet size distribution during non-cavitating and cavitating flows, the Sauter mean diameter (SMD) was calculated from the measured droplet diameters.

For droplet velocity calculations, 300 pairs of successive frames were selected. These frame pairs were selected in such a way that none of them shared the same droplets. After processing the frames and determining the location of the same droplet on each frame of the pairs, the displacement of the droplet was found and used to obtain the velocity of the droplet. Figure 5 shows typical locations of two different droplets in two successive frames, which were used for velocity calculations. After finding the displacement of the droplets, the velocity could be easily calculated using the time step of the image capturing experiments. Another code was developed in MATLAB 2018a to find the velocity of droplets. For all the selected pressures, the spray visualization for droplet calculations was performed at exactly the same location so that the results could be comparable. In this study, only  $x$  and  $y$  components of the velocity of the droplets were calculated, and the velocity in the  $z$  direction

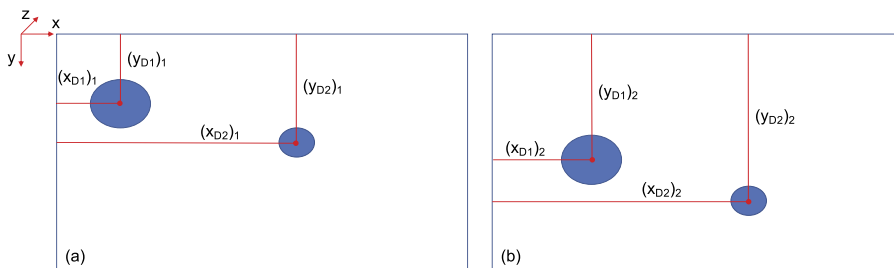


**FIG. 5.** Location of two different droplets in two successive frames: (a) frame 1, (b) frame 2 (D1: droplet 1, D2: droplet 2). Note: The time difference between the frames is approximately 41.5  $\mu$ s.

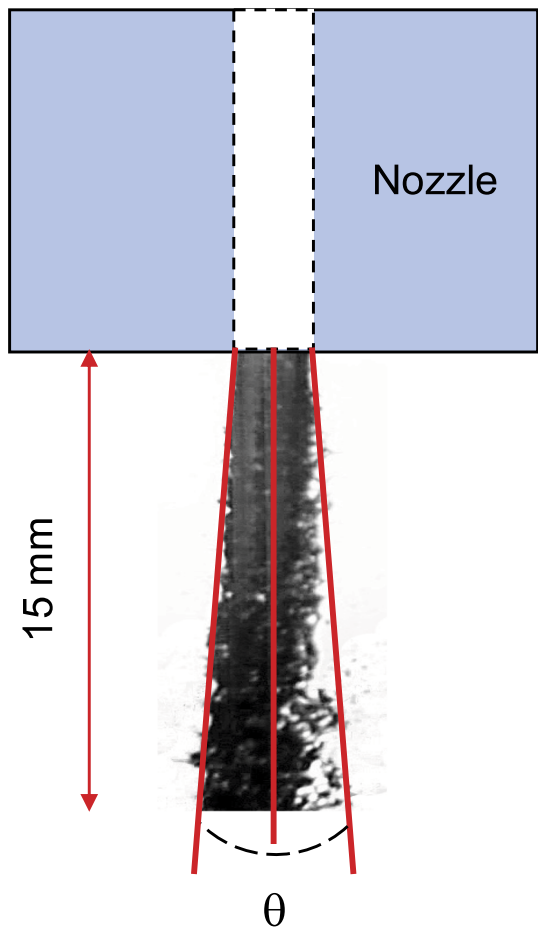


FIG. 6. Spray cone angle ( $\theta$ ).

for the recognized droplets in the selected frames was considered to be zero. The selection of the frames for velocity studies was made in such a way that the same droplet could be recognized in two successive frames with the same size. However, if the droplets have a

slight velocity in the  $z$  direction, the same droplet might not be recognized in the second frame. This method of frame selection for velocity studies ruled out many captured images. Since the nozzle has a symmetrical circular cross-section, it is valid to assume that if we consider all the droplets,  $x$  and  $z$  components of the droplet velocities will be approximately the same.

Spray cone angles of the liquid jets were measured from the captured images in the proximity of the nozzle exit (15 mm downstream the nozzle exit, similar to the study of Sou *et al.*<sup>12</sup>). For each injection pressure, 20 frames of the liquid jets with a time difference of approximately 5 ms were used to determine the spray angle as shown in Fig. 6, and the average of the 20 measured angles was reported as the spray cone angle at each injection pressure. The method presented in the study of Ghorbani *et al.*<sup>38</sup> was implemented to measure the spray cone angles.

III. RESULTS AND DISCUSSION

A. Flow regimes

Flow regimes for the case of water in the nozzle with an inner diameter of 0.9 mm are shown in Fig. 7. For cavitation numbers ( $\sigma$ ) greater than 1.086, no cavitation bubbles are observed inside the nozzle, and the liquid jet outside the nozzle forms a “wavy jet.” For the cavitation number of 1.086 ( $P = 690$  kPa), cavitation bubbles appear around the edge of the nozzle entrance. The inception inside the nozzle switches to developed cavitation at the cavitation number of 1.069. The transition from inception to developed cavitation is very quick, which implies that the cavitation bubbles could reach to the end of the nozzle within a short time after the cavitation inception. In the developed cavitating flow regime, the liquid outside the nozzle still has the form of the “wavy jet.” With a further increase in the injection pressure, the flow inside the channel becomes supercavitation, where the cavitation region inside the nozzle is extended to near the nozzle exit ( $1.059 < \sigma < 1.069$ ). Under supercavitation conditions, enhanced atomization of the liquid jet can be seen, which causes the formation of more droplets and ligaments. This morphology of the liquid jet is named “spray”, which has a wider angle compared to the “wavy jet.” For injection pressures higher than 1725 kPa, the nozzle flow exhibits hydraulic flip behavior, where the formation of the “flipping jet” outside the nozzle is observed.

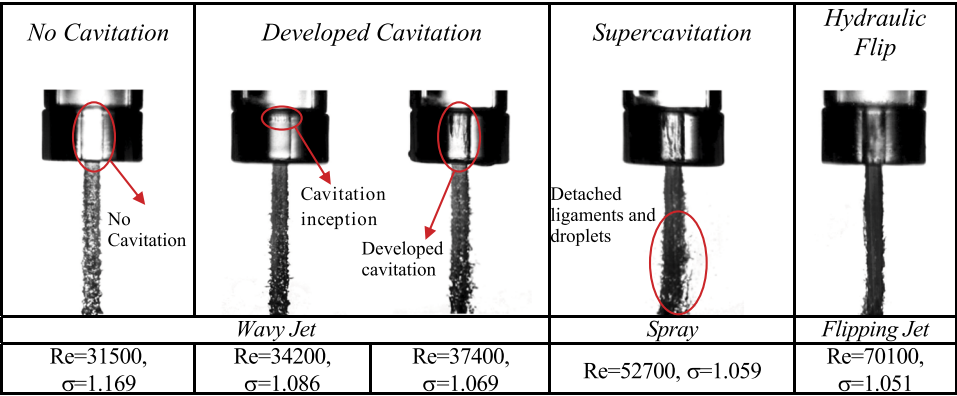


FIG. 7. Cavitating flow development inside the circular transparent quartz tube with a nozzle diameter of 0.9 mm for water.



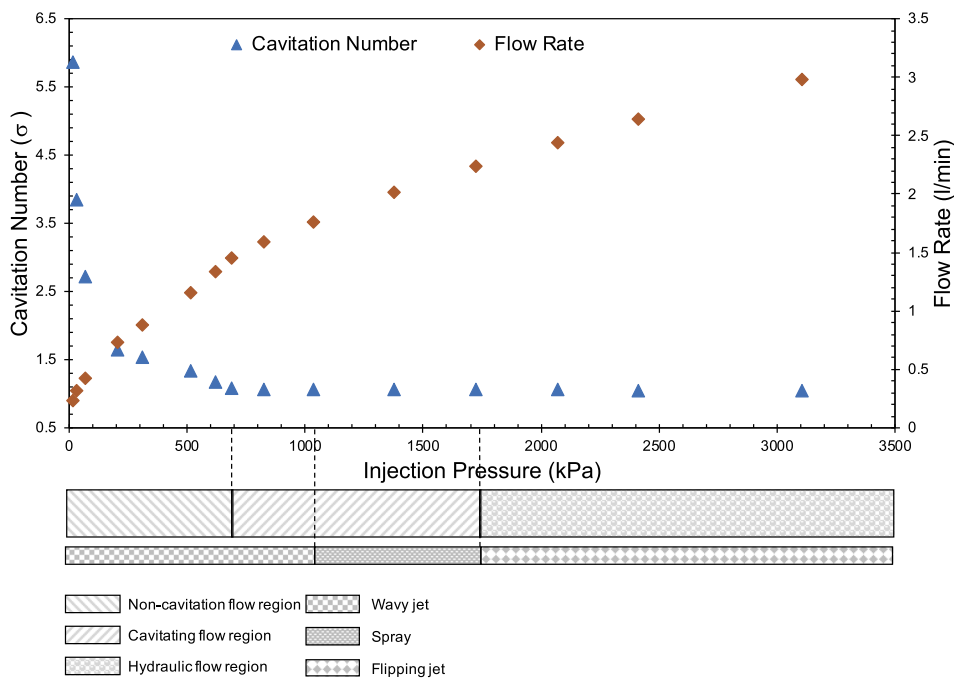


FIG. 8. Different flow regimes and flow rate in the nozzle at different injection pressures.

Before reaching cavitating flow conditions, the flow inside the nozzle is turbulent. At high injection pressures (>690 kPa), the generated cavitation bubbles could reach the region of the nozzle exit, which causes a wider cone angle. In the hydraulic flip regime, the cavitation bubbles extend to the exit of the nozzle without being attached to the channel wall. In this case, the cone angle could even be lower than the angle corresponding to the cavitation inception case. The hydraulic flip happens when the cavitation bubbles move to the end of the nozzle, and the air flow existing at the outlet at the atmospheric pressure fills one of the boundaries of the nozzle. As a result, the air passage enters the nozzle causing backflow. This flow pattern is rarely observed in the cavitation studies and is useful in different industrial applications such as hydroentangling.

Sou *et al.*<sup>12,19</sup> and Suh and Lee<sup>11</sup> used 2D rectangular and cylindrical nozzles to study the effect of cavitating flows on spray characteristics of injected flows. For these studies, the nozzles were of conventional scales. In the present study, despite the circular cross section of the nozzle and a much smaller diameter of the nozzle, the captured images of the development of cavitating flows at different injection pressures could be clearly visualized. As can be seen in Fig. 7, at the microscale, the cavitation bubbles fill a significant portion of the nozzle, leading to a lower liquid flow rate from the nozzle exit. After cavitation inception, increasing injection pressure leads to a higher volume fraction of cavitation bubbles, which suggests that small differences in cavitation numbers are experienced between cavitation inception and hydraulic flip conditions.

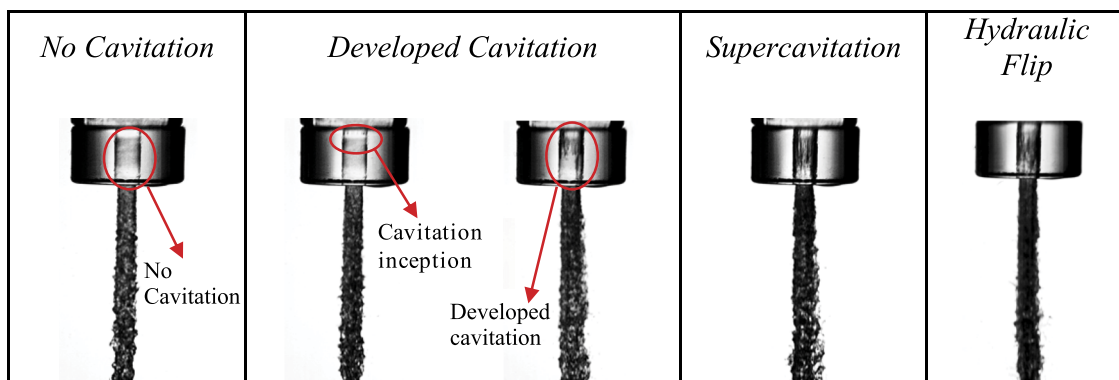


FIG. 9. Cavitating flow development inside the circular transparent quartz tube with a nozzle diameter of 0.9 mm with roughened surface for working fluid of PVA MB suspension.

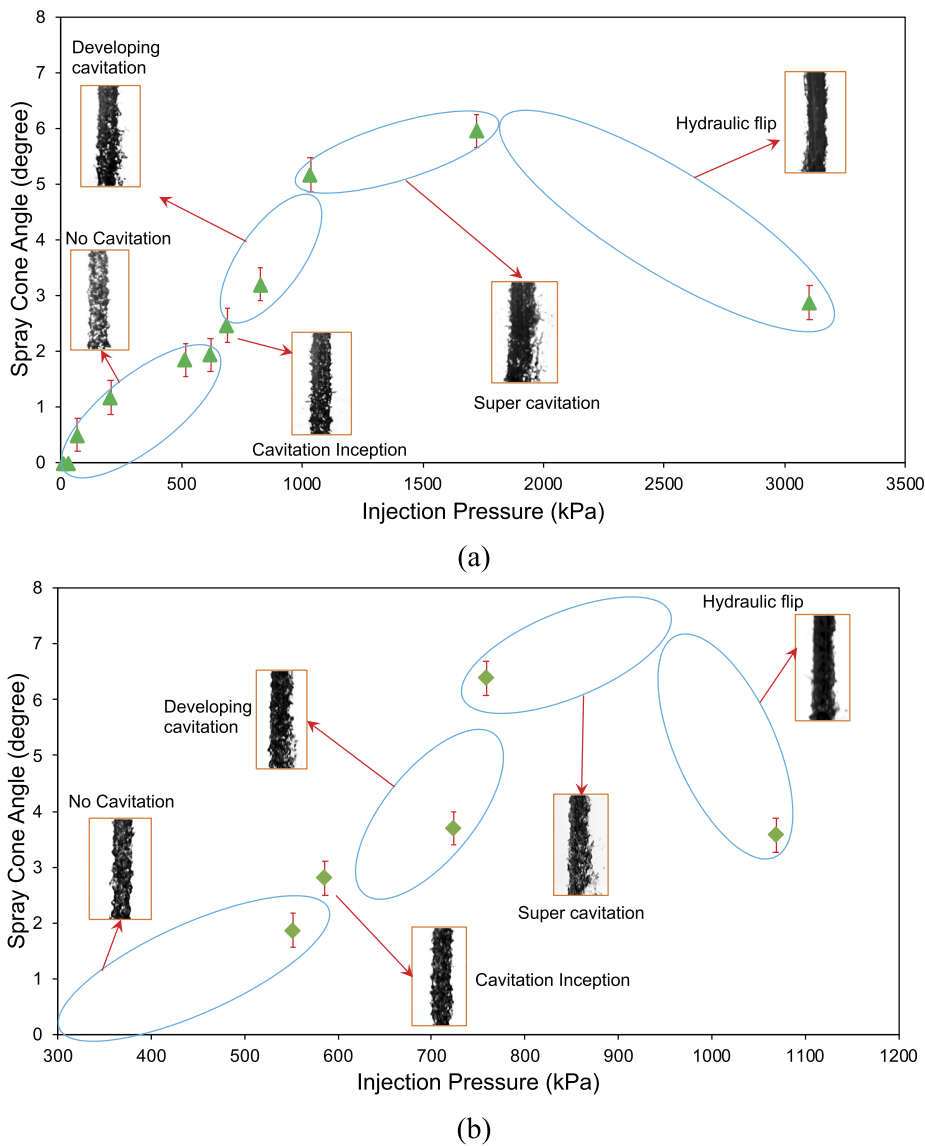
**TABLE IV.** Comparison of the injection pressures for different flow regimes.

	Water (nozzle without roughness) (kPa)	PVA MBs (nozzle with roughness) (kPa)
No cavitation	—690	—590
Cavitating flow	690–1725	590–1070
Hydraulic flip	1725	1070

Figure 8 shows the effect of the injection pressure on the liquid flow rate and cavitation number. As can be seen, an increase in the injection pressure results in higher liquid flow rates. The flow rate increases sharply at low injection pressures compared to higher injection pressures until the hydraulic flip region, at which the flow rate starts to rise more steeply. This behavior is demonstrated in

Fig. 8, as the cavitation number is inversely proportional to the square of the liquid velocity. In addition, Fig. 8 demonstrates different regimes of liquid jets. As mentioned before, both non-cavitation and developed cavitation flow regions correspond to wavy jet flows, while supercavitation forces the jet to acquire the spray form. The spray velocity increases aggressively after supercavitation, which is depicted in the flow rate profile beyond the injection pressure of 1035 kPa. This fact implies that the discharge has a significant effect on the flow pattern in the hydraulic flip region.

After recording different flow regimes corresponding to various injection pressures in the case of water, the second set of experiments was conducted for PVA MB suspensions using the quartz tube with a roughened nozzle. Figure 9 presents flow regimes inside the nozzle for the second set of experiments. The stages of development of cavitating flows are similar to that in the case of water in the nozzle without roughness. In Table IV, the injection pressures corresponding to

**FIG. 10.** Measured cone angles. (a) Working fluid of water (nozzle without roughness). (b) Working fluid of PVA MB suspensions (nozzle with roughness).



**FIG. 11.** Droplet recognition during the image processing using MATLAB<sup>™</sup> 2018a software. (a) Raw image, (b) threshold image, and (c) final processed image with boundaries for each recognized image.

different flow patterns for water inside the nozzle without roughness and PVA MB suspension inside the nozzle with roughened surface are compared. In the case of PVA MB suspension, cavitation incepts at the injection pressure of 590 kPa, which is 100 kPa lower than that in the case of water. As can be seen in Table IV, for working fluid of PVA MB suspension, the injection pressure range for cavitating flows is 590–1070, which is smaller compared to the cavitating flow range of 690–1725 kPa in the case of water. In the case of PVA MBs, the injection pressures corresponding to cavitation inception, supercavitation, and hydraulic flip flows are 590 kPa, 760 kPa, and 1070 kPa, respectively, which shows a decrease of 100 kPa, 275 kPa, and 655 kPa for the same flow regimes in the case of water. Moreover, PVA MBs result in enhanced atomization characteristics, which will be discussed later. Therefore, PVA MB suspension has the potential in intensifying the cavity clouds with the consideration of the surface and geometrical characteristics. Our previous study proves that the pressure can be reduced to much smaller values (below to the vapor saturation pressure) in the case of PVA MB suspension.<sup>26</sup> This characteristic causes an earlier arrival of different patterns of the cavitation compared to that in the case of water. The flow pattern transitions to supercavitation conditions at 1070 kPa in the case of PVA MBs, which is a comparatively low injection pressure for engineering and industrial applications.

## B. Spray cone angle

The spray cone angles for water and PVA MB suspensions were averaged and plotted against the injection pressure in Fig. 10. According to Fig. 10(a), at very low values of injection pressures, water liquid jet is completely flat and has a cone angle of  $0^\circ$ . With an increase in the injection pressure, waves start to appear on the liquid jet and raises the cone angle ( $0^\circ < \theta < 2^\circ$ ). At a pressure of 690 kPa, which corresponds to the cavitation inception, the spray cone angle begins to increase at a higher rate until the pressure of 1725 kPa at which the hydraulic flip region makes the cone angle drop at a considerable rate. To observe the effect of PVA MBs on the cone angle, the same approach was implemented to measure the spray cone angle of the liquid jet of PVA MBs. As can be seen in Fig. 10(b), the measured cone angles of PVA MB liquid jet have a similar trend as in the case of water. As mentioned in Sec. III A, for PVA MBs, cavitation incepts at a lower pressure, which leads to a steep increase in the spray cone angle at a lower pressure compared to the case of water. Although the measured cone angle of PVA MBs is bigger than in the case of water, there is not any considerable difference between the spray cone angles of water and PVA MB suspensions. According to Fig. 10, the largest spray cone angle was under supercavitation conditions in the cases of both water and PVA MB suspensions. Under supercavitation conditions, the cavitation bubbles could reach near the nozzle exit region, and the collapse of these bubbles causes a significant energy release, which results in

the detachment of more droplets from the mother jet leading to a larger spray cone angle.

## C. Atomization and droplet size distribution

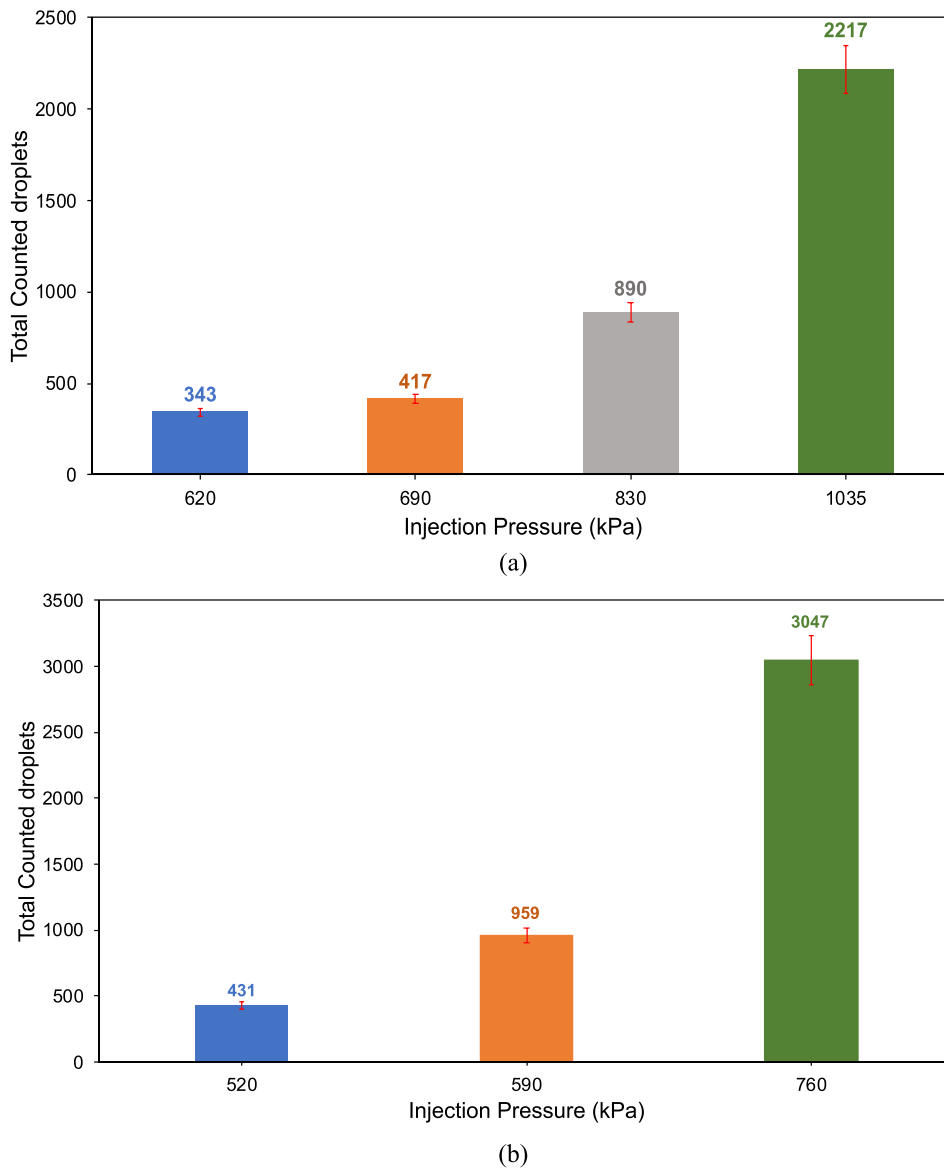
Figure 11 shows the steps of image processing for a sample frame and the recognized droplets by the developed in-house code after processing. As can be seen, the developed code has a high capability of spotting the droplets with an acceptable accuracy. A certain threshold was specified so that the method of counting the droplets on all of the pictures for all the pressures was the same.

Table V presents the selected pressures to study the influence of cavitation on atomization and droplet size distribution. As mentioned before, since the results in the case of water proved that supercavitation plays a predominant role in spray atomization, and due to quick transition to supercavitation after cavitation inception, the atomization study was not performed for developed cavitation in the case of PVA MB suspension inside the roughened nozzle. The images captured during the spray visualization of mentioned pressures were used for droplet recognition and to determine the droplet size distribution, which was utilized to reveal the effect of cavitation on spray characteristics of water and PVA MB suspension.

Figure 12 shows the effect of cavitation on total droplet numbers. In the case of water, there is not any considerable increase between counted droplets of non-cavitation and cavitation inception flow regimes. However, when the flow inside the nozzle becomes developed cavitation, there is a significant rise in the droplet number. As can be seen in Fig. 12(a), there is a substantial increase in the droplet number for the supercavitation flow pattern, which underlines the importance of this flow regime in atomization characteristics of the spray. According to Fig. 12(b), before cavitation inception, there is not any noticeable change in the total number of droplets in the case of PVA MB suspension compared to that in the case of water. However, for cavitating flows, the total droplet number significantly increases, which proves the beneficial impact of PVA MBs and surface roughness in droplet break-up and improving the atomization characteristics of cavitating flows, in addition to lowering the pressure required to incept the cavitating flow inside the nozzle.

**TABLE V.** Selected pressures to capture the images of the spray for droplet size and velocity determination.

	Water (kPa)	PVA MBs suspension (kPa)
Non-cavitating flow	620	520
Cavitation inception	690	590
Developed cavitation	830	...
Supercavitation	1035	760

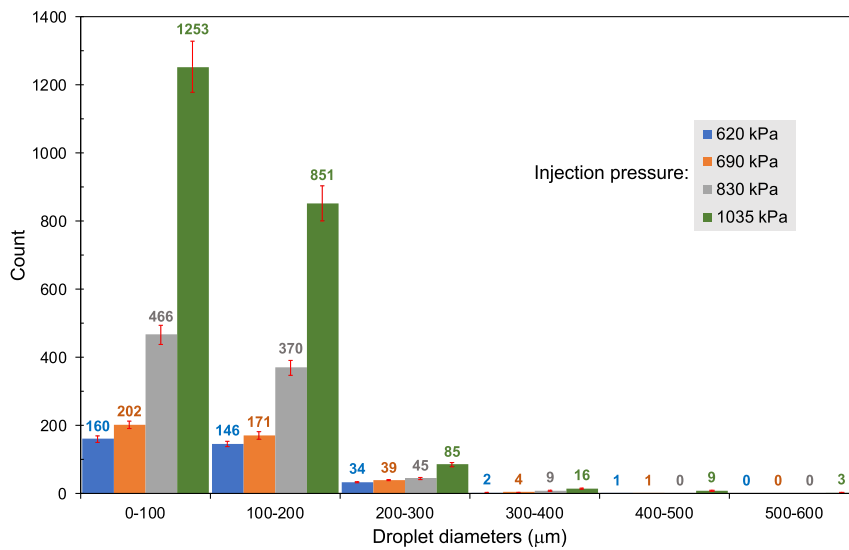


**FIG. 12.** Effect of cavitation on total counted droplets. (a) Total counted droplets for working fluid of water (nozzle without roughness). (b) Total counted droplets for working fluid of PVA MB suspension (nozzle with roughness).

Figure 13 displays the droplet size distribution for non-cavitating flow and different stages of cavitating flows. According to Fig. 13(a), in the case of water, the percentage of droplets with diameter smaller than  $200\ \mu\text{m}$  increases considerably for supercavitation flows compared to non-cavitation flows (89.2% for non-cavitation and 94.9% for supercavitation). In the case of PVA MB suspension [Fig. 13(b)], even though the percentage of droplets with diameter smaller than  $200\ \mu\text{m}$ , noticeably, increases during non-cavitation flows compared to water (from 89.2% to 97.4%), it is roughly the same during supercavitation flows for both cases (94.9% for water and 95.2% for PVA MB suspension). This outcome indicates the effect of the PVA MB suspension on increasing the quality of the spray atomization. As a result, larger impact pressures produced by the MB suspension lead to reduction in the liquid jet

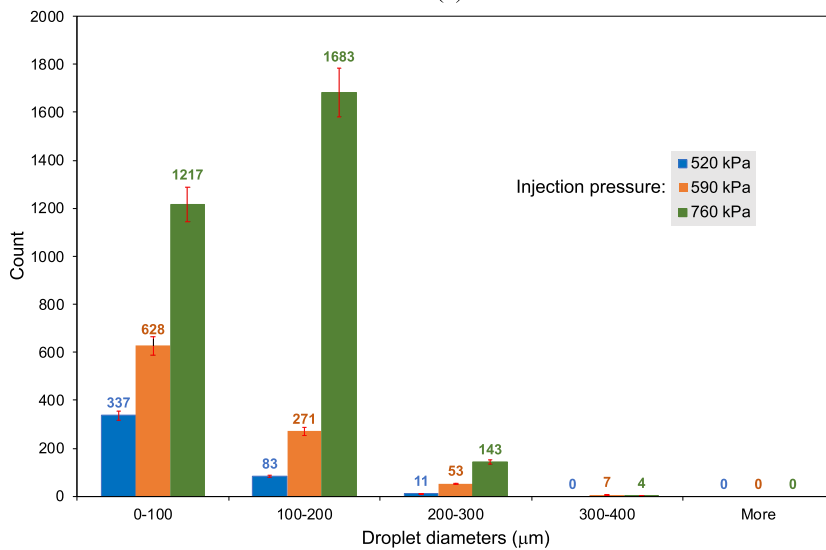
length and smaller droplet sizes during the primary and secondary breakups.<sup>26</sup>

Figure 14 presents the overall SMD distributions for non-cavitating and cavitating flows. As shown, for both water and PVA MB suspension, the SMD for cavitating flow is lower than that for non-cavitating flow, which implies the dominant role of cavitation in enhancing the atomization. This is due to the high energy release and localized shock waves from bubble collapse, which leads to fine atomization. When the collapse of cavitation bubbles happens, the energy stored on the surface of cavitation bubbles is converted into divergent breakup energy, which leads to enhanced atomization. As can be seen in Fig. 14(b), the overall SMD of PVA MB suspension is noticeably lower compared to the SMD of water for both non-cavitation and cavitating flow conditions,

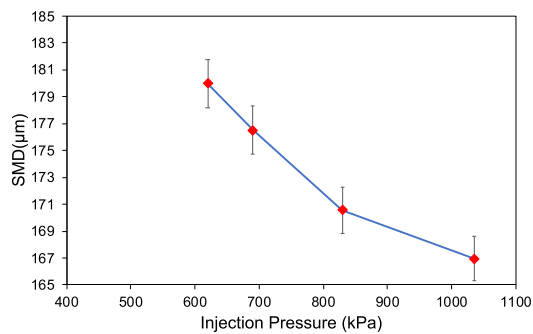


(a)

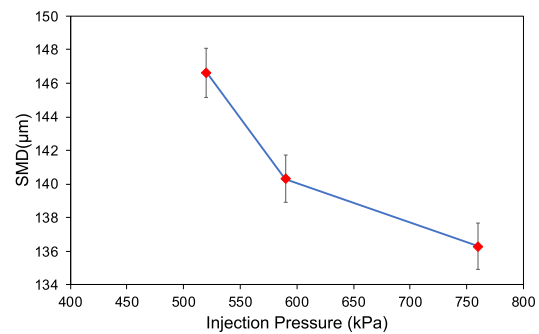
**FIG. 13.** Effect of cavitation on droplet size distribution. (a) Droplet size distribution for working fluid of water (nozzle without roughness). (b) Droplet size distribution for working fluid of PVA MB suspension (nozzle with roughness).



(b)



(a)



(b)

**FIG. 14.** Effect of cavitation on overall SMD. (a) Water (nozzle without roughness). (b) PVA MB suspension (nozzle with roughness).



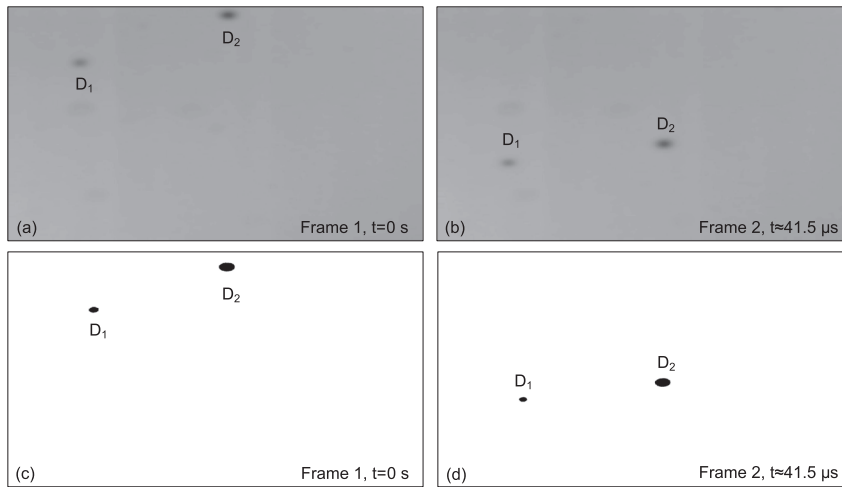


**FIG. 15.** Raw and processed images to locate the droplets on two successive frames. (a) and (b) Raw images; (c) and (d) respective processed images.

which suggests the intensified liquid atomization as a result of using PVA MBs.

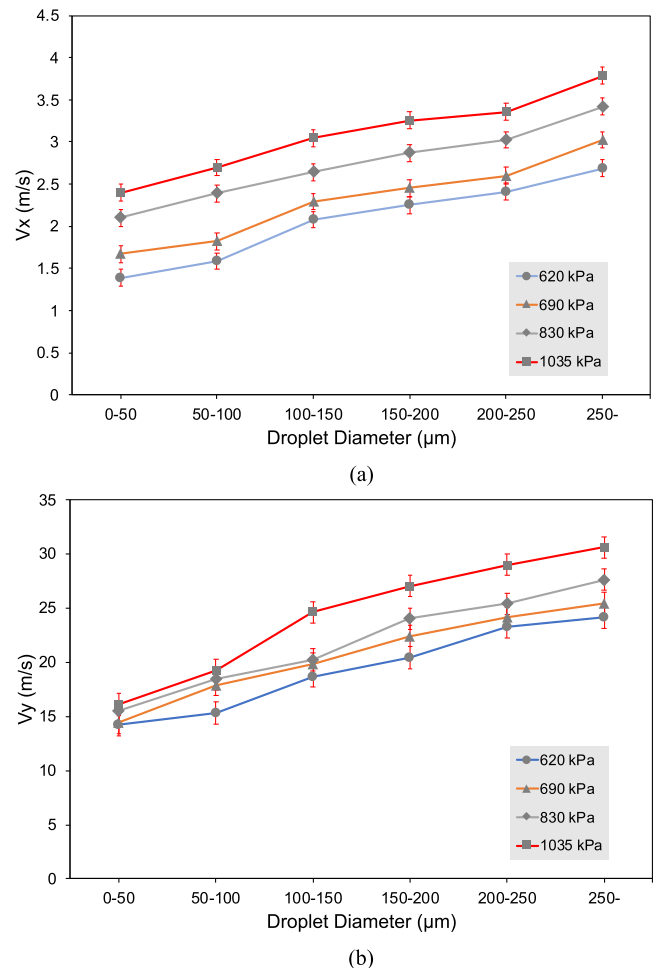
#### D. Droplet velocity distribution

Figure 15 shows an example of two successive frames processed by the developed code in MATLAB 2018a, which were used to find the locations of the droplets in each frame so that the velocity of the droplets could be calculated based on the method explained in Sec. II E.

After performing the same image processing on all the selected frames, the extracted data were used to find the velocity of the droplets. Figures 16(a) and 16(b) exhibit the water droplet velocities in x and y directions, respectively, for all the injection pressures presented in Table V. Increasing the injection pressure results in higher liquid flow rates leading to larger velocities of the injected liquid jet. The velocity of droplets in the x direction is much lower than that in the y direction, which indicates the low spray cone angle. As can be seen in Fig. 16(a), after cavitation inception, the distance between velocity trendlines increases compared to the distance between the velocity trendlines before cavitation inception (620 kPa and 690 kPa trendlines), which is the reason for the steep increase in the spray cone angle upon cavitation inception in Fig. 10(a). From Figs. 16(a) and 16(b), it can be noted that during supercavitation, both x and y components of the velocity of droplets increase considerably. This implies that the supercavitation flow inside the nozzle plays a dominant role in enhancing spray atomization besides making the spray have a larger cone angle.

Suh and Lee<sup>11</sup> used a phase Doppler particle analyzer to measure the velocity at the nozzle exit as well as the velocity of the droplets. They presented mean droplet velocities for turbulent flows, cavitating and flipping jet flow regions. The trend and increasing rate of the velocity of the droplets in different flow regions in this study are consistent with the results of their study.

The velocity fluctuations of the droplets with different diameters are shown as range bars in Fig. 16 (also included in Fig. 17). Velocity fluctuations range from  $\sim 0.05$  to  $\sim 0.15$  m/s in the x direction and from  $\sim 0.5$  to  $\sim 1.5$  m/s in the y direction.



**FIG. 16.** Velocity distribution of the departed droplets from the water jet immediately before and during cavitating flow inside the nozzle. (a) Velocity of the droplets in x direction. (b) Velocity of the droplets in y direction.

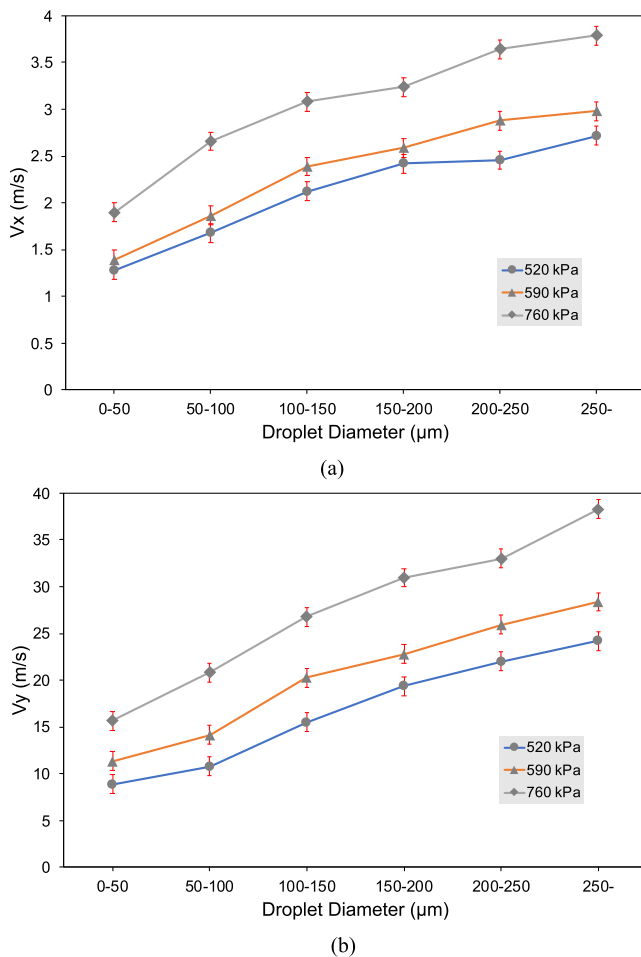


**FIG. 17.** Velocity distribution of the departed droplets from the PVA MB suspension jet immediately before and during cavitating flow inside the roughened nozzle. (a) Velocity of the droplets in x direction. (b) Velocity of the droplets in y direction.

Figure 17 presents x and y components of the droplet velocity in the case of PVA MBs in the roughened nozzle, respectively. The magnitude and trend in the velocity of the suspension droplets in the x direction are similar to those of water droplets in the x direction. Nonetheless, there is a minor increase in the magnitude, which explains the larger spray cone angle of PVA MB suspension compared to water. Comparing the y components of the velocity of the suspension droplets with water droplets in the cavitating flow regime, it can be realized that there is a considerable increase in the velocity of the droplets in the y direction for the PVA MB suspension droplets. The y component of the droplets in the case of PVA MBs could reach as high as approximately 40 m/s at an injection pressure of 760 kPa, while this value is nearly 30 m/s at an injection pressure of 1035 for the case of water. It can be deduced that the presence of PVA MBs not only results in lowering the required injection pressure for the development of cavitation flow in the nozzle, it also leads to a higher rate of atomization with larger velocities at lower pressure.

#### IV. CONCLUSIONS

In this study, a transparent quartz nozzle with an inner diameter of 0.9 mm was utilized to visualize cavitating flows of water inside the nozzle and investigate the effect of cavitation on spray atomization characteristics in terms of count, size, and velocity of the droplets. Another series of experiments were performed using a suspension of PVA MBs in a nozzle with modified surfaces to intensify cavitation and examine its influence on the spray. The obtained conclusions are as follows:

1. Cavitating flows inside the cylindrical nozzle can be classified into the following regimes: (1) non-cavitation flow, (2) developed cavitation, (3) supercavitation, and (4) hydraulic flip.
2. In the case of water, the injection pressures corresponding to cavitation inception, supercavitation, and hydraulic flip are 690 kPa, 1035 kPa, and 1725 kPa, respectively. Using PVA MBs lowers the injection pressure for the same flow regimes by 100 kPa, 275 kPa, and 655 kPa, respectively.
3. At the microscale, there is not any noticeable difference in the cavitation numbers corresponding to cavitation inception and hydraulic flip flow condition.
4. Cavitating flow increases the spray cone angle considerably, while using PVA MBs does not have any significant effect on the spray cone angle. In the hydraulic flip regime, the spray cone angle drops and it could have a value even smaller than that corresponding to cavitation inception.
5. For both cases of water and PVA MB suspension, cavitation enhanced the droplet count. The number of counted droplets in the case of PVA MBs is higher compared to that in the case of water, which proves the important effect of PVA MBs and modified surface on enhancing atomization characteristics of sprays. Supercavitation increases the percentage of droplets with smaller diameter than 200 μm from 89.2% to 94.9% in the case of water. This percentage for supercavitation flow is 95.2%, which is roughly the same as in the case of water. Cavitating flow lowers the overall SMD noticeably for both cases, and the overall SMD is smaller in the case of PVA MBs compared to that in the case of water.
6. Supercavitating flow has a significant influence on increasing the velocity of droplets. In the case of PVA MBs, in the supercavitation regime, the y component of the velocity of droplets is larger compared to that in the case of water.

#### ACKNOWLEDGMENTS

This work was supported by TUBITAK (The Scientific and Technological Research Council of Turkey) Support Program for Scientific and Technological Research Project (Grant Nos. 118S040 and 217M869) and the Sabanci University Internal Project Grant (Grant No. I.A.CF-18-01877). Equipment utilization support from the Sabanci University Nanotechnology Research and Applications Center (SUNUM) is gratefully appreciated.

#### REFERENCES

- 1 W. Bergwerk, "Flow pattern in diesel nozzle spray holes," *Proc. Inst. Mech. Eng.* **173**, 655–660 (1959).
- 2 C. Mishra and Y. Peles, "Cavitation in flow through a micro-orifice inside a silicon microchannel," *Phys. Fluids* **17**, 013601 (2005).

- <sup>3</sup>C. P. Egerer, S. Hickel, S. J. Schmidt, and N. A. Adams, "Large-eddy simulation of turbulent cavitating flow in a micro channel," *Phys. Fluids* **26**, 085102 (2014).
- <sup>4</sup>M. Jia, M. Xie, H. Liu, W.-H. Lam, and T. Wang, "Numerical simulation of cavitation in the conical-spray nozzle for diesel premixed charge compression ignition engines," *Fuel* **90**, 2652–2661 (2011).
- <sup>5</sup>F. Payri, V. Bermúdez, R. Payri, and F. J. Salvador, "The influence of cavitation on the internal flow and the spray characteristics in diesel injection nozzles," *Fuel* **83**, 419–431 (2004).
- <sup>6</sup>R. Payri, J. M. García, F. J. Salvador, and J. Gimeno, "Using spray momentum flux measurements to understand the influence of diesel nozzle geometry on spray characteristics," *Fuel* **84**, 551–561 (2005).
- <sup>7</sup>B. Abderrezzak and Y. Huang, "A contribution to the understanding of cavitation effects on droplet formation through a quantitative observation on breakup of liquid jet," *Int. J. Hydrogen Energy* **41**, 15821–15828 (2016).
- <sup>8</sup>F. Liu, Z. Li, Z. Wang, X. Dai, X. He, and C.-F. Lee, "Microscopic study on diesel spray under cavitating conditions by injecting fuel into water," *Appl. Energy* **230**, 1172–1181 (2018).
- <sup>9</sup>J. Cui, H. Lai, K. Feng, and Y. Ma, "Quantitative analysis of the minor deviations in nozzle internal geometry effect on the cavitating flow," *Exp. Therm. Fluid Sci.* **94**, 89–98 (2018).
- <sup>10</sup>R. Payri, F. J. Salvador, J. Gimeno, and O. Venegas, "Study of cavitation phenomenon using different fuels in a transparent nozzle by hydraulic characterization and visualization," *Exp. Therm. Fluid Sci.* **44**, 235–244 (2013).
- <sup>11</sup>H. K. Suh and C. S. Lee, "Effect of cavitation in nozzle orifice on the diesel fuel atomization characteristics," *Int. J. Heat Fluid Flow* **29**, 1001–1009 (2008).
- <sup>12</sup>A. Sou, S. Hosokawa, and A. Tomiyama, "Effects of cavitation in a nozzle on liquid jet atomization," *Int. J. Heat Mass Transfer* **50**, 3575–3582 (2007).
- <sup>13</sup>M. T. Shervani-Tabar, S. Parsa, and M. Ghorbani, "Numerical study on the effect of the cavitation phenomenon on the characteristics of fuel spray," *Math. Comput. Modell.* **56**, 105–117 (2012).
- <sup>14</sup>M. Ghorbani, G. Alcan, A. K. Sadaghiani, A. Mohammadi, M. Unel, D. Gozuacik, and A. Koşar, "Characterization and pressure drop correlation for sprays under the effect of micro scale cavitation," *Exp. Therm. Fluid Sci.* **91**, 89–102 (2018).
- <sup>15</sup>R. Payri, F. J. Salvador, J. Gimeno, and L. D. Zapata, "Diesel nozzle geometry influence on spray liquid-phase fuel penetration in evaporative conditions," *Fuel* **87**, 1165–1176 (2008).
- <sup>16</sup>S. Som, A. I. Ramirez, S. K. Aggarwal, A. L. Kastengren, E. El-Hannouny, D. E. Longman, C. F. Powell, and P. K. Senecal, "Development and validation of a primary breakup model for diesel engine applications," Document No. 2009-01-0838, 2009.
- <sup>17</sup>W. H. Nurick, "Orifice cavitation and its effect on spray mixing," *J. Fluids Eng.* **98**, 681–687 (1976).
- <sup>18</sup>F. Örley, T. Trummer, S. Hickel, M. S. Mihatsch, S. J. Schmidt, and N. A. Adams, "Large-eddy simulation of cavitating nozzle flow and primary jet break-up," *Phys. Fluids* **27**, 086101 (2015).
- <sup>19</sup>A. Sou, M. I. Maulana, S. Hosokawa, and A. Tomiyama, "Ligament formation induced by cavitation in a cylindrical nozzle," *J. Fluid Sci. Technol.* **3**, 633–644 (2008).
- <sup>20</sup>Z. He, W. Zhong, Q. Wang, Z. Jiang, and Z. Shao, "Effect of nozzle geometrical and dynamic factors on cavitating and turbulent flow in a diesel multi-hole injector nozzle," *Int. J. Therm. Sci.* **70**, 132–143 (2013).
- <sup>21</sup>Z. He, Z. Shao, Q. Wang, W. Zhong, and X. Tao, "Experimental study of cavitating flow inside vertical multi-hole nozzles with different length–diameter ratios using diesel and biodiesel," *Exp. Therm. Fluid Sci.* **60**, 252–262 (2015).
- <sup>22</sup>J. M. Desantes, R. Payri, F. J. Salvador, and J. De la Morena, "Influence of cavitation phenomenon on primary break-up and spray behavior at stationary conditions," *Fuel* **89**, 3033–3041 (2010).
- <sup>23</sup>P. G. Aleiferis, J. Serras-Pereira, A. Augoye, T. J. Davies, R. F. Cracknell, and D. Richardson, "Effect of fuel temperature on in-nozzle cavitation and spray formation of liquid hydrocarbons and alcohols from a real-size optical injector for direct-injection spark-ignition engines," *Int. J. Heat Mass Transfer* **53**, 4588–4606 (2010).
- <sup>24</sup>J. Serras-Pereira, Z. Van Romunde, P. G. Aleiferis, D. Richardson, S. Wallace, and R. F. Cracknell, "Cavitation, primary break-up and flash boiling of gasoline, iso-octane and n-pentane with a real-size optical direct-injection nozzle," *Fuel* **89**, 2592–2607 (2010).
- <sup>25</sup>A. K. Agarwal, S. Som, P. C. Shukla, H. Goyal, and D. Longman, "In-nozzle flow and spray characteristics for mineral diesel, Karanja, and Jatropa biodiesels," *Appl. Energy* **156**, 138–148 (2015).
- <sup>26</sup>M. Ghorbani, H. Chen, L. G. Villanueva, D. Grishenkov, and A. Koşar, "Intensifying cavitating flows in microfluidic devices with poly (vinyl alcohol) (PVA) microbubbles," *Phys. Fluids* **30**, 102001 (2018).
- <sup>27</sup>M. Ghorbani, A. S. Aghdam, M. T. Gevari, A. Koşar, F. Ç. Cebeci, D. Grishenkov, and A. J. Svagan, "Facile hydrodynamic cavitation ON CHIP via cellulose nanofibers stabilized perfluorodroplets inside layer-by-layer assembled SLIPS surfaces," *Chem. Eng. J.* **382**, 122809 (2020).
- <sup>28</sup>A. S. Aghdam, M. Ghorbani, G. Deprem, F. Ç. Cebeci, and A. Koşar, "A new method for intense cavitation bubble generation on layer-by-layer assembled slips," *Sci. Rep.* **9**, 11600 (2019).
- <sup>29</sup>R. Xue, Y. Ruan, X. Liu, F. Cao, and Y. Hou, "The influence of cavitation on the flow characteristics of liquid nitrogen through spray nozzles: A CFD study," *Cryogenics* **86**, 42–56 (2017).
- <sup>30</sup>D. Li, S. Liu, Y. Wei, R. Liang, and Y. Tang, "Numerical investigation on transient internal cavitating flow and spray characteristics in a single-hole diesel injector nozzle: A 3D method for cavitation-induced primary break-up," *Fuel* **233**, 778–795 (2018).
- <sup>31</sup>F. Cavallieri, A. El Hamassi, E. Chiessi, G. Paradossi, R. Villa, and N. Zaffaroni, "Tethering functional ligands onto shell of ultrasound active polymeric microbubbles," *Biomacromolecules* **7**, 604–611 (2006).
- <sup>32</sup>A. Bhattacharya and P. Ray, "Studies on surface tension of poly (vinyl alcohol): Effect of concentration, temperature, and addition of chaotropic agents," *J. Appl. Polym. Sci.* **93**, 122–130 (2004).
- <sup>33</sup>Sigma-Aldrich, Poly(vinyl alcohol), version 6.2 safety data sheet, revised 18 January 2015.
- <sup>34</sup>M. Okazaki, K. Shioda, K. Masuda, and R. Toei, "Drying mechanism of coated film of polymer solution," *J. Chem. Eng. Jpn.* **7**, 99–105 (1974).
- <sup>35</sup>S. V. V. N. Kothapalli, V. Daeichin, F. Mastik, L. A. Brodin, B. Janerot-Sjöberg, G. Paradossi, N. de Jong, and D. Grishenkov, "Unique pumping-out fracturing mechanism of a polymer-shelled contrast agent: An acoustic characterization and optical visualization," *IEEE Trans. Ultrason., Ferroelectr., Freq. Control* **62**, 451–462 (2015).
- <sup>36</sup>D. Grishenkov, C. Pecorari, T. B. Brismar, and G. Paradossi, "Characterization of acoustic properties of PVA-shelled ultrasound contrast agents: Linear properties (part I)," *Ultrasound Med. Biol.* **35**, 1127–1138 (2009).
- <sup>37</sup>F. Cavallieri, A. El Hamassi, E. Chiessi, and G. Paradossi, "Stable polymeric microballoons as multifunctional device for biomedical uses: Synthesis and characterization," *Langmuir* **21**, 8758–8764 (2005).
- <sup>38</sup>M. Ghorbani, G. Alcan, M. Unel, D. Gozuacik, S. Ekici, H. Uvet, A. Sabanovic, and A. Kosar, "Visualization of microscale cavitating flow regimes via particle shadow sizing imaging and vision based estimation of the cone angle," *Exp. Therm. Fluid Sci.* **78**, 322–333 (2016).